# EFFECTS OF PHOTO OXIDATION ON THE MECHANICAL BEHAVIOR OF POLYMERIC MATERIALS: AN EXPERIMENTAL STUDY

By

Abd-Elrahman Korayem

A THESIS

Submitted to
Michigan State University
in partial fulfillment of the requirements
for the degree of

Civil Engineering—Master of Science

2021

ABSTRACT

EFFECTS OF PHOTO OXIDATION ON THE MECHANICAL BEHAVIOR OF POLYMERIC MATERIALS: AN EXPERIMENTAL STUDY

By

Abd-Elrahman Korayem

Here, an experimental study is carried out to understand the degradation of crosslinked polymeric materials by exposure to coupled thermo- and photo-oxidation, and their effects on mechanical behavior of the material. Our investigation specifically focuses on two cured elastomeric adhesives: (i) a silicon-based and (ii) a polyurethane-based adhesive. Samples were prepared and subjected to UV radiation at three different temperatures namely 45, 60 and 80°C, for different aging periods ranging from 1 to 150 days. Chemical damage is characterized by the FTIR, DSC and Swelling tests which help us to monitor the change in the chemical composition of the materials along the aging durations and conditions. Mechanical damage is characterized by uniaxial tensile failure test, cyclic tensile test and permanent set test. These tests revealed the change of behavior of our materials along the aging periods and conditions. The changes in mechanical behavior vary depending on the material, aging temperature and duration. We show that behavior of the materials aged in the photo-oxidative environment is in fact a result of a combination of two separable modes of damage, Mechanical and Environmental. Accordingly, We are able to further separate the environmental damage mode into one created by the effects of temperature and another created by the combination of temperature and radiation. This separability has been confirmed with a Neo-hookean model, which proved that for a combined state of aging such as photo-oxidation the material cannot be characterized by models which consider only single modes of damage. Such regimes would require approaches such as the micro-mechanical approach to fully consider the effects by all the damage modes found in complex aging phenomena.

TABLE OF CONTENTS

LIST OF TABLES

LIST OF FIGURES

# 1. INTRODUCTION

Due to excellent thermal and chemical resistance of polymers, they are abundantly used in various applications(Bower, 2002). However, long time exposure to a variety of environmental conditions along with mechanical damages can cause severe damage to polymer structure and limits its performance over time (Mohammadi et al., 2020). This process is often referred to as *aging*. Major types of aging are thermo-oxidative (Mohammadi and Dargazany, 2019), hygrothermal (Nachtane et al., 2019), hydrolysis (Bahrololoumi et al., 2020) and photo-oxidative aging (Rodriguez et al., 2020).

Over the lifetime of polymeric materials, photo-oxidative aging becomes a continuous risk to the performance of equipment and structures that are subjected to UV radiation such as that present in sunlight(Geuskens and David)(Blaustein and Searle, 2013). With the growing use of polymers in nearly every application in our daily lives(Chandra and Rustgi), photo-oxidation becomes an ever more pressing issue for the sustainable use of polymers in their working environments over extended periods of time (Namazi, 2017). Elastomers are a special class of polymers with a highly nonlinear constitutive behaviour, which makes their photo-oxidative deterioration much harder to predict than a linearly behaving material (Rezig et al., 2020). Given the complex molecular structures that can emerge from aging and the countless effects additives could have on the unaged and aged material, achieving a robust framework for behavior prediction can be a great challenge. Additionally, polymeric substances can react differently to photo-oxidation when mixed together or with other additives that are used as fillers or curing agents(Bigg, 1987)(Khabbaz et al., 1999) (Liu et al., 2020). This adds a further challenge for achieving a generalized form for characterizing elastomers. In elastomers, polymer chains consist mainly of a variety of cross-linked hydrocarbon chains that are bonded together either through physical bonds forming as hydrogen bonds or chemical bonds forming as covalent bonds(Flory, 1953)(Hiemenz and Lodge, 2007).

A UV ray carries sufficient energy to cause photolytic degradation of the C-C backbone or

cross-links between the carbon chains(Biron, 2015)(Grossman and Gouzman, 2003). This is most apparent at shorter wavelengths, which are characterized by having higher energy and is sufficient to cause degradation(Andrew R. George, 2008). This in turn destabilizes the compound and increases it's reactivity, allowing for rapid oxidation and deterioration of the bonds that hold the structure of the polymer matrix intact(Tolinski, 2015). The deterioration can cause significant changes to the mechanical characteristics of polymeric materials, which may be very damaging to the performance of equipment and parts if not considered (Feldman, 2002). Accordingly, higher energy UV spectra coming from shorter wavelengths found in sunlight, affect polymers the most(Biron, 2015), so the amount of expected damage to polymeric components due to photo-oxidation must be considered for products designed for outdoor applications. Another phenomena that must also be considered is thermo-oxidation, as UV radiation from sunlight is accompanied with infrared radiation which is experienced by bodies as heat(Bhatia).

Thus for a given application involving UV light and heat, we find that polymers can be affected through two main mechanisms, i) the damage caused by the heat energy and/or that of UV radiation, which releases free radicals into the matrix, and ii) Oxidation, which occurs due to oxygen in the environment reacting with the free radicals released (Audouin et al., 1998). The presence of free-radicals from the heat or UV energy have a destabilizing effect on the matrix, thus each mode of damage has an amplifying effect on the other, which causes further damage to the material. Accordingly, for any full characterization of the actual deterioration that occurs in polymeric materials, it is crucial that investigative efforts focus on the combination of photo-thermal aging instead of simply photo induced aging.

Previous studies on the topic usually focus on the general behavior of the aged material, along with the evolution of certain chemical properties of interest for characterization, such as in the case of Signor et al(Signor et al., 2003), Pickett(Pickett, 2017), Dupuis et al(Dupuis et al., 2017) and Wu et al(Wu et al., 2020). Other focuses were directed towards using the Arrhenius functions which were based on activation energies for predicting shift factors for time-temperature super po-

sition and kinetic studies, as in the case of (Cruz-Pinto et al., 1994), (Liu et al., 2018), (Zaghdoudi et al., 2020) and (Rezig et al., 2020). Most studies on thermo-oxidation or photo-oxidation can be categorized into two groups i) characterizing the chemical response to correlate the chemical variations to the mechanical variation, or ii) developing an empirical approach to construct a master curve which is extremely difficult in case of coupled thermo-radiative aging due to convoluted degradation path(Celina, 2013)(Gillen et al., 1997) . Even though Both systems might function for a certain material or a given aging condition, they cannot be used for generating a generalized form for all materials in a certain category, such as elastomers. This is due to the variability in chemical composition and micro-structure between materials, which in turn influences their response to different environmental and mechanical stresses(McKeen, 2018)(Rubinstein and Colby, 2003). A further complexity arises from the high variability in materials' capacity for diffusion limited oxidation(DLO) due to the differences in their spatial heterogeneity in oxidative degradation. This disparity affects their capacity for oxygen diffusion into the matrix and consumption during photo-thermo induced oxidative aging, which makes the accurate prediction of the products of the oxidation from a chemical perspective more complex (Quintana and Celina, 2018). (Gillen et al., 2000) showed that there exists a synergism between mechanical loading and the amount of potential environmental damage that can occur in a sample. This shows, that while both of these modes of damage act on different aspects of the material, they potentially have a complementary effect that must be isolated in order to properly characterize the materials of interest.

A solution to this issue can be found in micro-mechanical modelling, as instead of trying to fit a single equation to all materials, a more discrete approach is performed. This method involves only considering the general effect of each aging factor on a single micro-structural component of the material and then compounding it up-til the bulk structure (Sadd, 2018). Accordingly, to improve the effectiveness and accuracy of the formulation created for a certain aging type, it is necessary to investigate which individual aging factors contribute the most to the behavior of the material(Mohammadi and Dargazany, 2018)(Bahrololoumi et al., 2019 (in submission).

In this study, we investigate the mechanism of damage accumulation for materials exposed to coupled mechanical and environmental damages modes, and which factors plays a more significant role on affecting the behavior of two elastomeric materials in each of those modes. Accordingly, we will study how to superpose mechanical damages such as deformation induced softening with environmental damage that is induced by couple thermal-radiative damage. We seek to verify our hypothesis through experimental efforts which investigate the change in mechanical and chemical properties and behavior of the materials of this study. To investigate this separability the damage modes are hypothesized to operate on two distinct networks. A Network containing C-C chains, crosslinked together chemically. The other Network is devoid of chemical crosslinking and comprises of C-C chains only. A representation of this can be seen in Figure 1.

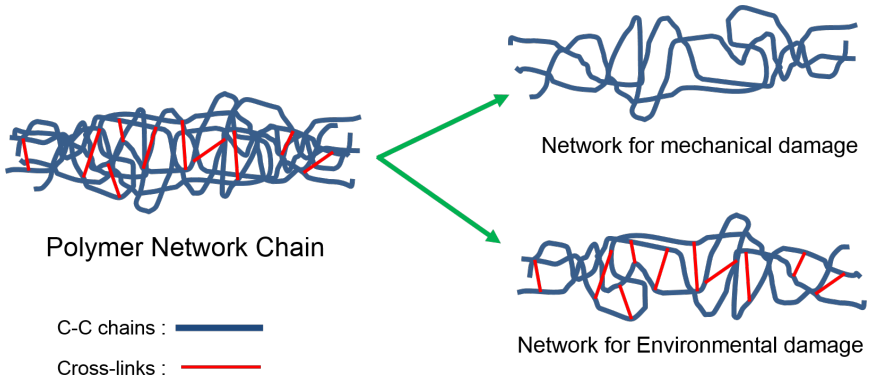


Figure 1: Full network shown broken down into sub-networks, each susceptible to a unique damage mode.

## 2. MATERIALS AND METHODOLOGY

The material selection process involved considering different variants of hard and soft polymers. Our greatest interest was in observing the change in elastic behavior of polymers and accordingly selecting materials with high visco-elastic properties was our prime interest. Different variations of silicon adhesive, acrylic, epoxy, polyurethane and other base compounds were investigated, aged and tested in the expected environmental and mechanical loading conditions that the study would expand on. Accordingly, we were able to narrow down the material list to four materials initially, then they were further reduced to two materials which were most representative of the behavior that would be useful to the study. The study focuses on two variants of elastomeric adhesives, namely silica-based and polyurethan based adhesives with properties given in Table 1.

Table 1: Properties of study materials

| **Hardness** | Soft | Softer |
|---|---|---|
| **Material** | Polyurethane adhesive (PUA) | Silicone Adhesive (SA) |
| **Un-Aged Shore Hardness** | 60 (A) | 32 (A) |
| **Un-Aged Modulus** | 3.2 MPa | 0.5 MPa |
| **Un-Aged Cured strength** | 7.6 MPa | 2.5 MPa |
| **Un-Aged Elongation at break** | 375 % | 680 % |

***Sample preparation*** was performed according to the ASTM D-412 (Standard, 2006). The samples were cast separately in a custom mold in contrast to being punched out of a single sheet. This is achieved by injecting the adhesive into the mold using a commercial applicator one cavity at a time. Excess material is then removed, and the samples are left to cure over a period of 5 days, after which they are removed from the mold using full-body holders to avoid mechanical damage prior to the aging process. To verify the optimal curing and avoid over-curing, the samples were

tested at different curing times, to which it was observed that behavior does not change beyond 5 days of curing in room temperature for up to 30 days. Samples were labelled, weighed, measured and photographed before and after the aging process to track any change that could occur to the materials due to photo-oxidation.

a)  b)  c) 

Figure 2: a) Mold used for casting of samples capable of producing 20 samples per batch, b) Labelled samples, c) Samples dimensions being taken.

**Aging environment:** The samples are separately aged in accordance to the ASTM G-151(Standard, 2019) at an irradiation of 1 W/m$^2$/ nm wavelength for three aging durations, 1, 10 and 30 days at three temperatures, 45, 60 $°C$ and 80 $°C$.The reasoning behind the temperature selection is that we required at least three distinct temperatures to monitor the behavior of the materials with increasing temperatures and investigate whether there is a trend to be witnessed or not. Thte QUV machine that we use for aging the samples has a minimum temperature setting of 45$^o$C and a maximum setting of 80$^o$C. The UV spectrum the samples were subjected to, was one generated by UVA-340 lamps that cover wavelengths ranging from 295 – 340 nm. These wavelength represent the greater portion of radiation intensity for sunlight, and accordingly are the most appropriate to use in the study of the photo-oxidative effects from sunlight(Feldman, 2002). In order to fully understand the effects pure photo-oxidation have on polymeric materials the samples that were aged at 45 $°C$ were additionally aged to 60 and 150-day periods. This will allow us to properly isolate the effects of photo-thermal oxidation experienced at the higher temperatures from those of pure photo-oxidation.

a)  b) 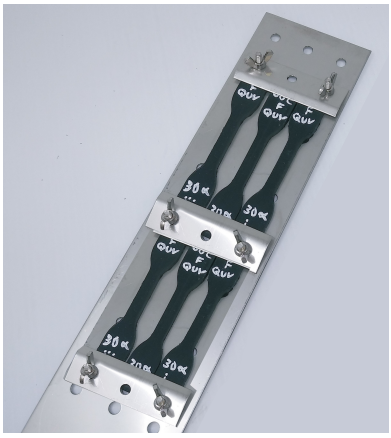

Figure 3: a) QUV machine used for aging, b) Modified adjustable sample size fixture created for our experiments.

Table 2: Aging temperatures and durations

| **Aging Temperature [°C]** | 45 | 60 | 80 |
|---|---|---|---|
| **Aging Duration [days]** | 1-10-30-60-150 | 1-10-30-60-150 | 1-10-30-60-150 |

## 2.1. TESTING

***Uniaxial Tensile tests*** were preformed to identify deterioration in material performance according aging environment. To achieve this, specially designed tensile tests were used to analyze the behavior of the samples, and were conducted at room temperature.

- *Failure test* where the samples are continuously stretched until failure, are performed to derive the constitutive behavior, ultimate strength $\sigma_f$, ultimate strain $\epsilon_f$, and toughness $T$.
- *Cyclic test @ increasing amplitude* were carried out to capture mechanical damages induced by stretch history $\lambda_{max}$. In essence, the test can capture the evolution of permanent set $e_1$, energy dissipation $\mathcal{D}$ with respect to $\lambda_{max}$. Four stretch amplitudes were chosen based on the initial failure test as shown in Table 3.

*All tensile tests were performed on a Test Resources Universal Testing Machine (UTM), Model 311-39 Dual Column Test Machine with a 2,250 lb (10 kN) capacity. The tests were also performed*

Table 3: Cyclic test strain limits

| **Material** | PUA | SA |
|---|---|---|
| **Strain Limits** | 112.5, 225, 337.5, 405 | 87.5, 175, 262.5, 315 |
| **Revised Strain Limits** | 35, 75, 112.5, 130 | 45, 87.5, 125, 175 |

*at 50 mm/min extension rate, which was determined experimentally to be the highest rate of loading to not have an effect on the behavior of the material*

a) 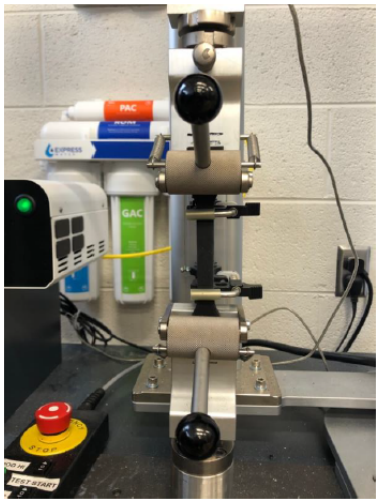

b) 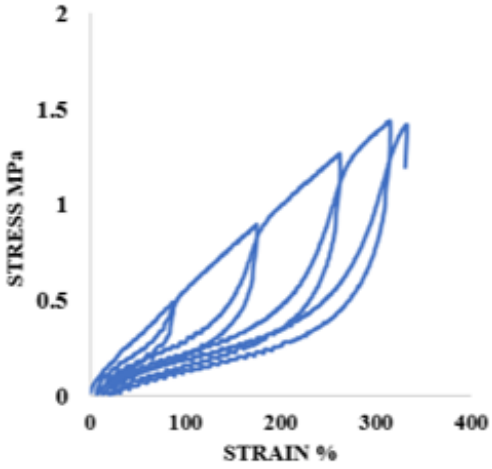


Figure 4: a) UTM machine used for testing along with roller grips used for soft material gripping, b) Cyclic test template with no repetition of cycle.

***Permanent set*** tests were designed and carried out to capture the evolution of $e_1$ the non-vanishing residual strain, as a measure of damage with respect to different environmental and mechanical loads. In those tests, virgin samples were initially stretched to 50% strain and held at that extension during aging condition as shown in Figure 5. The stretched samples were placed in the same aging conditions used for the mechanical testing for different periods. They were then subsequently removed after the periods had concluded, weighed and measured to inspect the residual and permanent strain which had developed.

Figure 5: Apparatus used to hold the samples at the desired strain during the aging period

***FTIR*** tests were conducted to characterize changes in chemical composition of the matrix in the course of photo-oxidative aging using a JASCO FTIR/IR 4000 series machine. Each material was scanned with a different refractive crystal and bandwidth due to the difference in transmittance properties between them. SA was scanned with a Diamond crystal under a bandwidth of 400-4000 $cm^{-1}$. PUA on the other hand was scanned with a Germanium crystal under a bandwidth of 600-4000 $cm^{-1}$ due to the significant noise it causes in the 400-600 $c\,m^{-1}$ range.

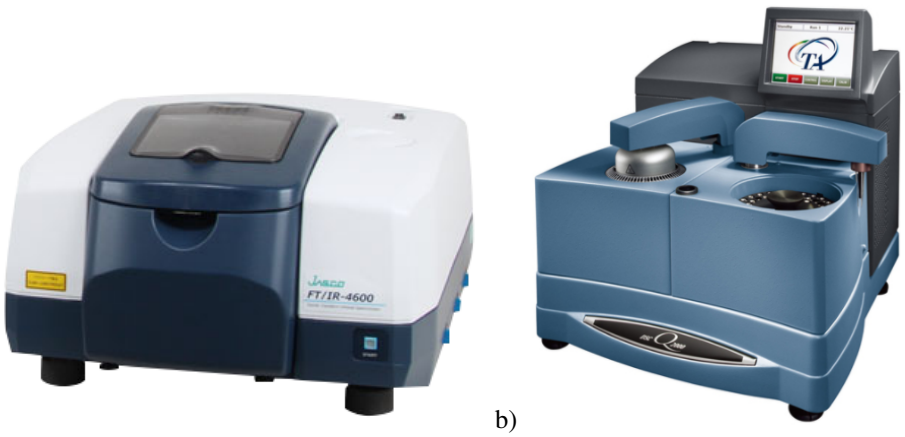


a) b)

Figure 6: a) FTIR scanning machine used, b) DSC Q2000 series machine.

***DSC test*** was performed on both materials to track the change in heat capacity and flow of the materials throughout the aging process. The test was conducted on a Q2000 series Differential Scanning Calorimetry machine from TA Instruments, with a temperature scan between $80^oC$ and $350^oC$ at a heating rate of $10^oC$/min. Small sections were cut from the aged samples and loaded in

the machine where a temperature sweep was performed on them. This test was conducted to give us insight into the behavior of the material across a wide array of temperatures and enables us to determine the glassification temperature for PUA along with the Endothermic melting temperature for SA considering that the glassification temperature for SA is estimated to be near -170$^oC$, which is too low and cannot be achieved in the DSC test.

**Swelling test** was performed to characterize the changes in the cross-link density of the matrix in the course of photo-oxidative aging by submerging the samples into three different solvents namely, Hexane, Toluene and Pentane until the polymer matrix is saturated with the solvent. The saturation limit is determined by the complexity and level of entanglement of the polymer matrix due to cross-linking.

## 2.2. Mechanical and environmental Damage

Damage induced by environmental and mechanical factors has an accumulating nature. This feature allows us to identify damage by tracing the incremental changes in the materials with respect to the aging durations and conditions. A major challenge, however, is to properly isolate the effects of different damage mechanisms on the constitutive behavior of the materials. Of particular interest is firstly to separate mechanical and environmental effects, and secondly to separate photo- and thermo-oxidation, which can be achieved through the selected conditions, as the effects of thermo-oxidation are least apparent at 45 °C and most apparent at 80 °C. Thermo-oxidative effects are well studied in literature and accordingly the effects of photo-oxidation can be more easily deduced. This can only be achieved however if there is a separability between the damage cause by mechanical stress from our tests and the damage.

## 3. RESULTS AND DISCUSSION

*Silicone Adhesive (SA):*

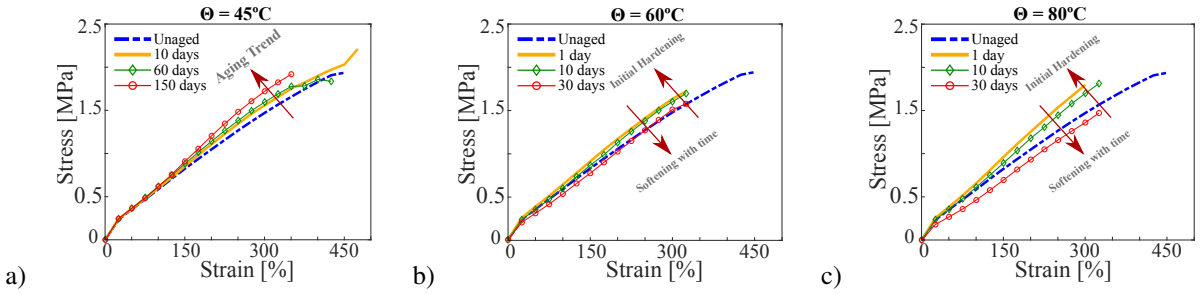


Figure 7: a) Failure test of SA aged at 45°C, b) 60°C, and c) 80°C for different aging periods.

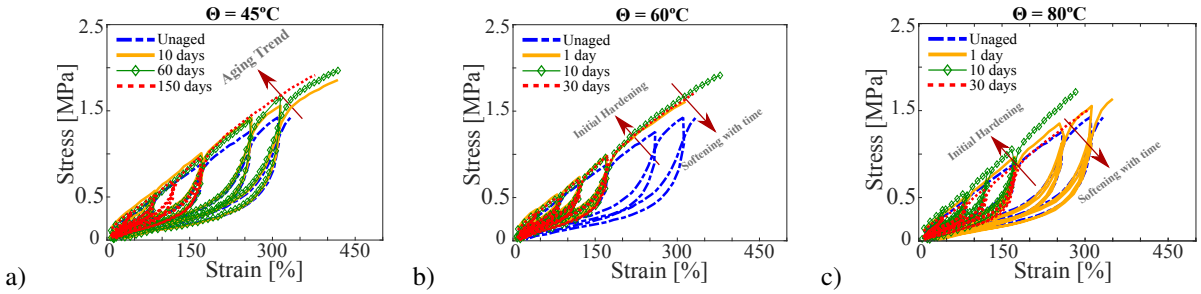


Figure 8: Cyclic tensile test at constant and increasing amplitudes for SA aged at a) 45°C, b) 60°C, and c) 80°C for different aging periods.

Results for the tensile failure tests of SA are presented in Figure 7 and 8, respectively.

The conditions the samples are being subjected to vary in both temperature and duration of exposure. Samples have a specific behavioral trend across the aging conditions, as samples exhibit continuous stiffening at 45°$C$, but at higher temperatures the material initially exhibits stiffening and then softens with longer aging periods. This behavior can be understood by considering aging as a competition between purely photo-oxidative effects and those of photo-thermal degradation.This can be seen through the lens of initial over-curing of the material, which peaks after a certain amount of energy is absorbed by the material to achieve full-curing, which is then followed directly by a phase of chain detachment sub-mechanism, which continues throughout the

remainder of the aging process(Bettina et al., 2017). This chain detachment, which is likely to be accompanied with a loss in cross-link density, decreases the ability of the material to resist mechanical loading and accordingly causes the material to become softer.

Ultimate strength and stain for silicon adhesive decreases regardless of aging duration, with the exception of samples aged at $45°C$ for 10 days, suggesting that the material is experiencing some form of over-curing up til this condition.

*PUA:*

Results for the failure and cyclic tests of PUA are presented in Fig.9 and 10, respectively.

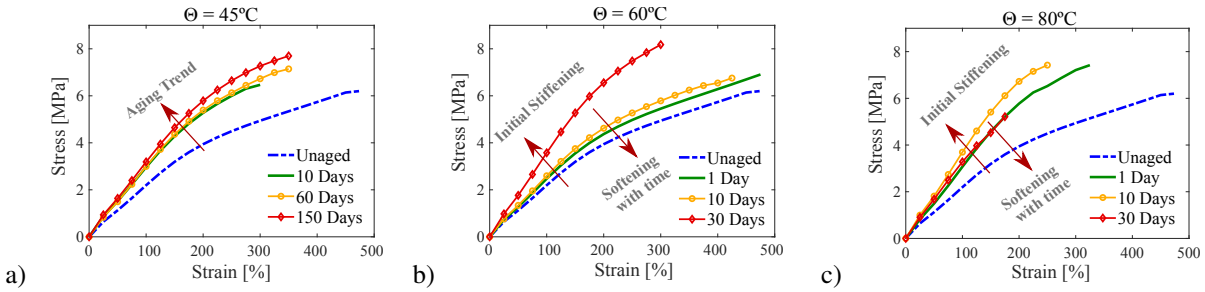


a) b) c)

Figure 9: a) Failure tensile test of PUA aged at 45°C, b) 60°C, and c) 80°C for different aging periods.

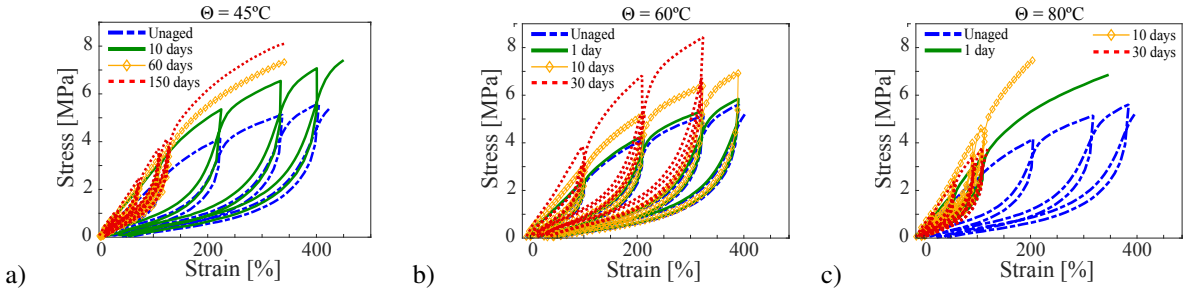


a) b) c)

Figure 10: a) Cyclic tensile test of PUA aged at 45°C, b) 60°C, and c) 80°C for different aging periods.

The material behaves similarly across all temperatures and durations with the exception of $80°C$ for 30 days where the material loses its intgrity and there is an unexpected softening effect

dominating the behaviour. Aging causes polyurethane to stiffen with time, increases ultimate strength, yet decreases the ultimate strain that the material can be extended to.

UV radiation increases the elastic modulus with the longer aging periods. As it can be seen at higher temperatures and longer aging durations, increased heat causes significant damage to the polymer as it loses it's mechanical properties. With the ultimate strength dropping from 6.4 MPa to 4.8 MPa, the ultimate strain from 490% to 170% and toughness as well as shown in Figure 12. Therefore, we can assume that the dual effect of photo-thermal aging has a softening effect induced by cross-link detachment in contrast to the single mode of thermo-oxidative aging as shown in (Al-Azhary et al., 2020), which shows that the same material exhibits a continuously hardening behavior at higher temperatures. This can be explained by considering that the combination of both heat and radiation contains the sufficient amount of energy to act on the cross-links and entangled chains causing scission, which limits the entanglements of the longer chains, causing the material to lose it's ability to resist mechanical loading. This energy or damage mode however, was not available in the case of pure photo-oxidation, which is dominant at lower temperatures.

## 3.1. Mechanical Damages in Aged samples

***Permanent Set*** results are shown in Figure 11 for samples aged at 1, 10 and 30 days at 45, 60 and 80°C.

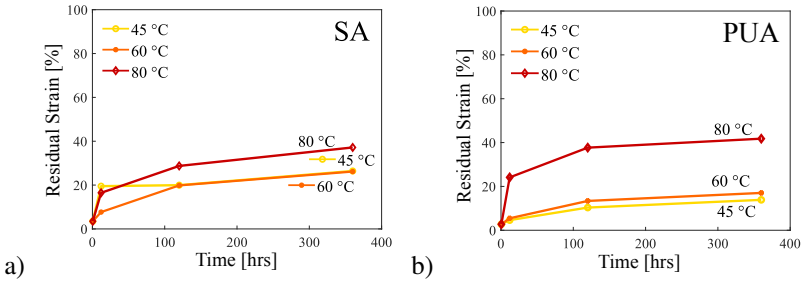


Figure 11: a) Permanent set results for SA strained continuously at 45, 60 and 80 °C. for different aging periods, b) Showing permanent set results for PUA strained continuously at 45, 60 and 80 °C. for different aging periods.

In both silicon and PU compounds, results show increasing permanent set $e_1$ for longer aging

periods, and higher temperatures, with almost similar behaviour between the samples aged at 45° and 60°C, and a clear difference with those aged at 80°C, which can suggest that the optimum operating temperatures for the materials should be below 60°C. Similar observations were made for increasing stretch amplitude $\lambda_{max}$ and number of cycles $n_c$, as summarized below

$$e_1 \propto \{T, t, \lambda_{max}, n_c\} \qquad \mathcal{D} \propto \left\{T, t, \lambda_{max}, \frac{1}{n_c}\right\} \tag{1}$$

The tests also show that the polymer chains and associated cross-links of the silicon adhesive (SA) have a relatively high level of thermal stability and are less likely to be damaged or significantly altered when subjected to thermal and mechanical stresses. On the other hand, PUA performance at higher temperatures suggests that either the compounds contains volatile components that when subjected to heat can dissipate and are replaced with less stable chains/cross-links, which causes the drop in material behavior observed at 80 °C.

**Ultimate strength $\sigma_f$ and strain $\epsilon_f$** continuously change in the course of aging which confirms changing the contribution of cross-linking formation and detachment at different stages of aging. Failure properties of the SA and PUA samples were shown in Figure 12 and 13, respectively. In general, one can see that the total toughness of the material $T$ decreases with respect to aging time, regardless of the behaviour of the $\sigma_f$ and $\epsilon_f$. At 45°C however, initial increase of toughness can be associated to over-curing, the effect of which gradually fades away.

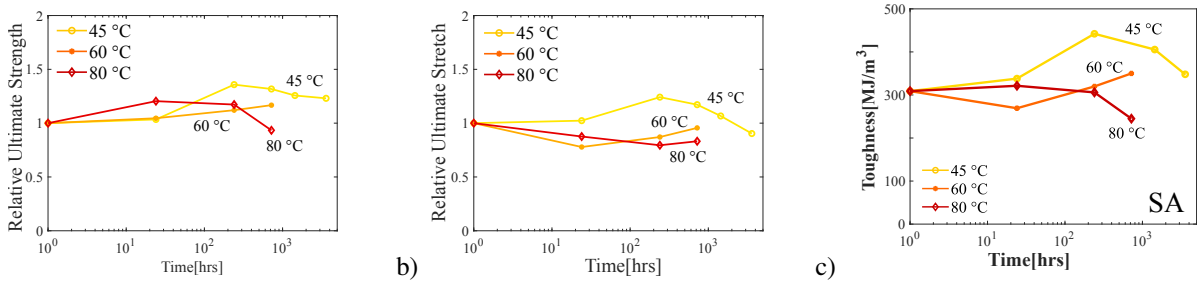


Figure 12: a) Change in ultimate strength of SA along time for the different aging temperatures of 45, 60 and 80 °C. b) Showing the change in ultimate stretch of SA along time for the different aging temperatures of 45, 60 and 80 °C.

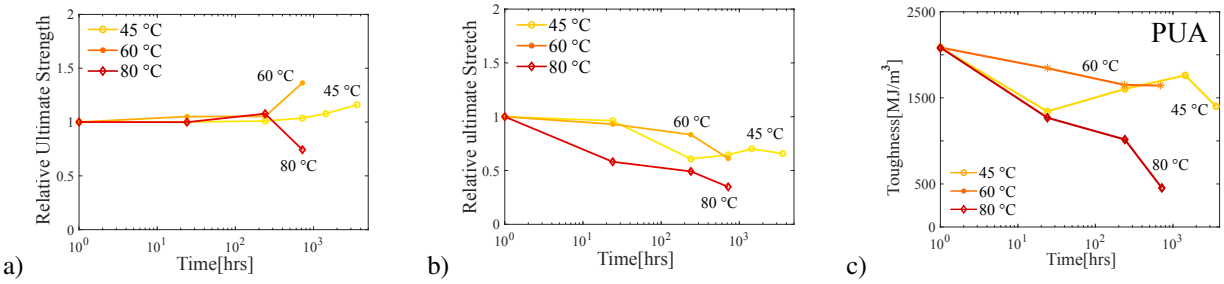


Figure 13: a) Change in ultimate strength of PUA along time for the different aging temperatures of 45, 60 and 80 °C. b) Showing the change in ultimate stretch of PUA along time for the different aging temperatures of 45, 60 and 80 °C.

## 3.2. Separation of Mechanical & Environmental damage

In order to validate the two chain theory's underlying framework, we need to prove that the change in the mechanical constitutive behavior of the materials stems from the damage sustained from the environmental damage, while the ratio could be sustained from mechanical damage is constant given that the mechanical loading regime remains unchanged. Accordingly, to separate the effects of mechanical and environmental damage in photo-oxidative aging on the performance of the polymers, we introduced three dimensionless parameters to describe the effect of environmental aging on mechanical performance obtained from cyclic and failure tests, namely $\sigma*$, $e*$ and $W*$.

These parameters represent the ratios of mechanical performance for the same criteria along the cyclic testing regime. They also eliminate the effect of the environmental damage, since they are not absolute values, but rather ratios within the same test, and accordingly each parameter is only compared to another which has sustained the same amount of environmental damage.

Relative softening in stress amplitude, $\sigma$*, is derived from cyclic tests @ constant amplitude with the following equation:

$$\sigma_n^* = \frac{\sigma_n}{\sigma_{max}} \tag{2}$$

where $\sigma_{\max}$ is the maximum stress achieved in the first cycle at a given strain, and $\sigma_n$ is the stress achieved at the nth cycle at constant stretch amplitude. As expected from elastomeric systems the largest decline is expected to occur in the first cycle, $\sigma_1^* > \sigma_n^*$ which gradually disappear in

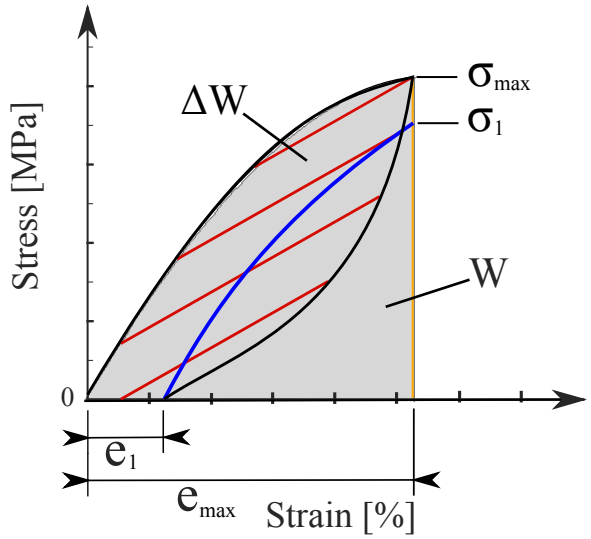


Figure 14: Different parameters being calculated from the cyclic test.

next cycles as can be seen in Figure 15. Hereafter, we will simply use $\sigma* := \sigma_1^*$ to represent the softening that occurs in the material as a result of mechanically damage through the ratio of retained strength to the original strength at a specific stretch amplitude, here the first stretch limit in the cyclic test $\lambda_1$.

The second parameter being calculated is the relative permanent set, $e^*$, which is calculated by

$$e_n^* = \frac{e_n}{\lambda_1} \tag{3}$$

where $\lambda_1$ is the stretch amplitude of the first set of cyclic tests, and $e_n$ is the permanent set of cycle $n$. Hereafter, we will simply use $e* := e_1^*$, as the strains used to make these calculations are denoted in Table 3 . This metric shows the evolution of permanent set from the first cycle as a percentage of that cycle's stretch amplitude and it indicates how much the material loses its overall elasticity with time. The third and final metric is the relative hysteresis loss($W*$), which is calculated by the following equation,

$$W^* = \frac{\mathcal{D}_n}{W} \tag{4}$$

Where $W$ is the total work done in extending the material in one cycle $\Delta W$, denoted in Eqn.4 as $D_n$, is the net work stored by the polymer. This metric allows a further understanding of the loss of elasticity induced by mechanical damage and how much the mechanical loss changes throughout the photo-oxidative aging period.

## 3.3. Observations

### 3.3.1. SA

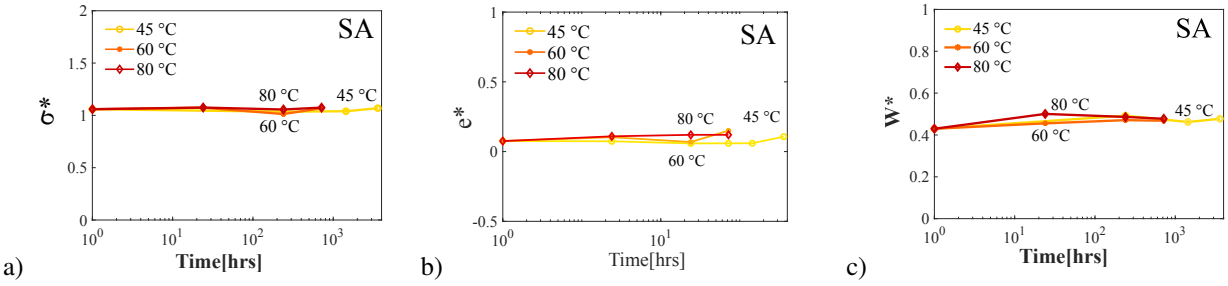


Figure 15: Changes a) in $\sigma$* across aging conditions at $\lambda_1$ in the cyclic test b)in $e^*$, and c) in W* during the first load cycle against aging time at $\lambda_1$ in the cyclic test.

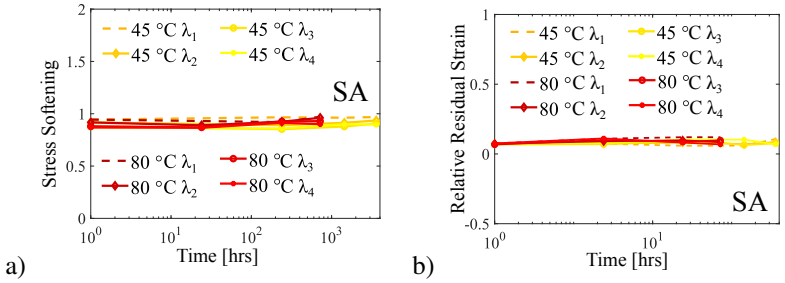


Figure 16: a) Stress softening across different cycles for SA at 45, 60 and 80 °C, where $\lambda_n$ is the stretch limit of cycle n in the cyclic test b) Showing relative residual strain across different cycles for SA at 45, 60 and 80 °C, where $\lambda_n$ is the stretch limit of cycle n in the cyclic test.

As can be seen from Figure 15, all three parameters of stress softening, relative residual strain and hysteresis loss in SA compound can be considered to be constant and independent of the temperature and aging time. This means that they are independent from the effects of environmental aging generally and environmental damage, which includes losses in stiffness and toughness,

specifically.

In order to ensure that the consistency in behavioral independence from environmental effects persists across the entirety of the mater tensile response, we removed the role of stretch amplitude by computing these parameters across the different strain peaks present in the cyclic test and we have shown that then results are consistent and similar at across all of them at high and low temperatures alike, as demonstrated in Figure 16.

### 3.3.2. PUA

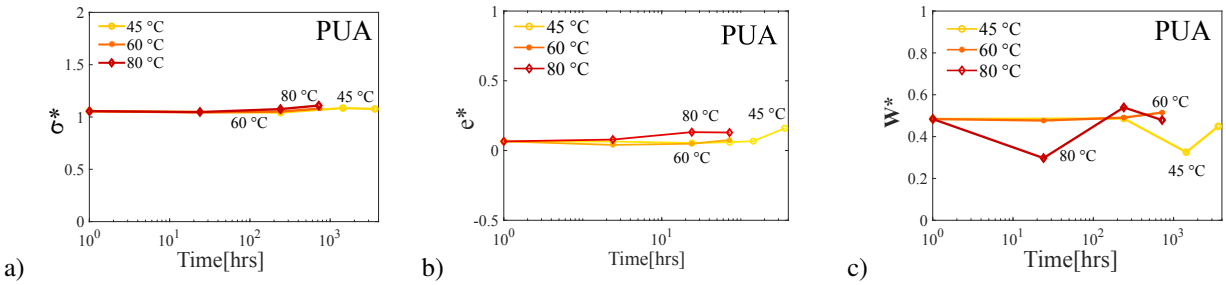


Figure 17: a) Change in values of $\sigma$* across aging conditions during the first cycle with time. b) Showing the change in $e^*$. c) Showing the change of the W* during the first cycle with time.

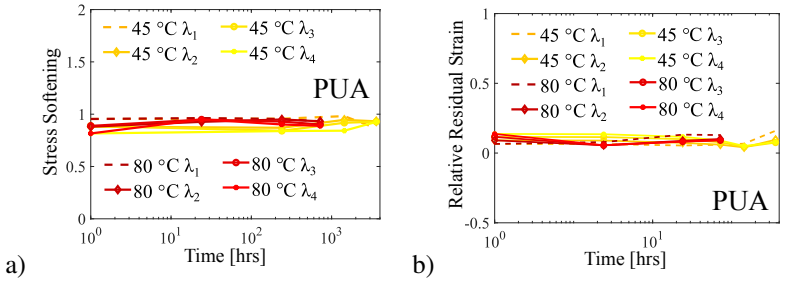


Figure 18: a) Stress softening across different cycles for PUA at 45, 60 and 80 °C, where $\lambda_n$ is the stretch limit of cycle n in the cyclic test b) Showing relative residual strain across different cycles for PUA at 45, 60 and 80 °C, where $\lambda_n$ is the stretch limit of cycle n in the cyclic test.

Similar results were obtained for PUA, as it does not exhibit any significant stress softening along both the aging period and time, as shown in Figure 17a). This performance however is not maintained in relative residual strain and hysteresis loss, which indicates that the material's elastic properties are changing with time and temperature. As can be seen in Figure 17b), the loss of

elasticity occurs gradually along the aging period and with increases in temperature similarly. No specific trend can be deduced however from from Figure 17c), however we can infer that there is a certain change that occurs for the amount of energy loss of each cycle with respect to time and temperature.

Both compounds exhibit similar behavior in stress softening across temperatures and aging duration for the different cycles, as shown in Figure 17 and 18. This indicates that both materials maintain a similar micro-structural assortment of chains, which unwind in the same manner regardless of the existing damage in the polymer matrix. Results also suggest that the there is no change in the recoil mechanism responsible for the elastic properties of the materials, but rather the main change that materials experience during aging is in the mechanism that is in action during the loading process. Accordingly, the damage that does occur from environmental factors does not affect the C-C backbone which gives the materials their elastomeric nature. Thus, the chain scission that does occur along the aging process cannot be considered must be acting mainly on chains which do not contribute to the elastic nature of the the materials. **The results show that the mechanical and environmental modes of damage can be considered separable in both compounds.**

The differences in behavior that occur in unloading indicates that the modes of damage are affecting the components responsible for creating the elastic nature of the materials. The behaviour is resulted from the competition between the detachment and reformation of c-c links, which is mostly controlled by the oxygen attack, diffusion rate and consumption rate(Rubinstein and Colby, 2003). This means that the differences in values of both the relative residual strain and hysteresis loss that occur along the aging durations and temperatures occur due to the different networks of crosslinks that are broken down and created throughout the aging process and during mechanical testing. Accordingly, since this damage mode is related to both environmental conditions and the mechanical loading case, the separability of these modes of damage becomes significantly less for the recoil/elastic behavior of the materials.

## 3.4. FTIR

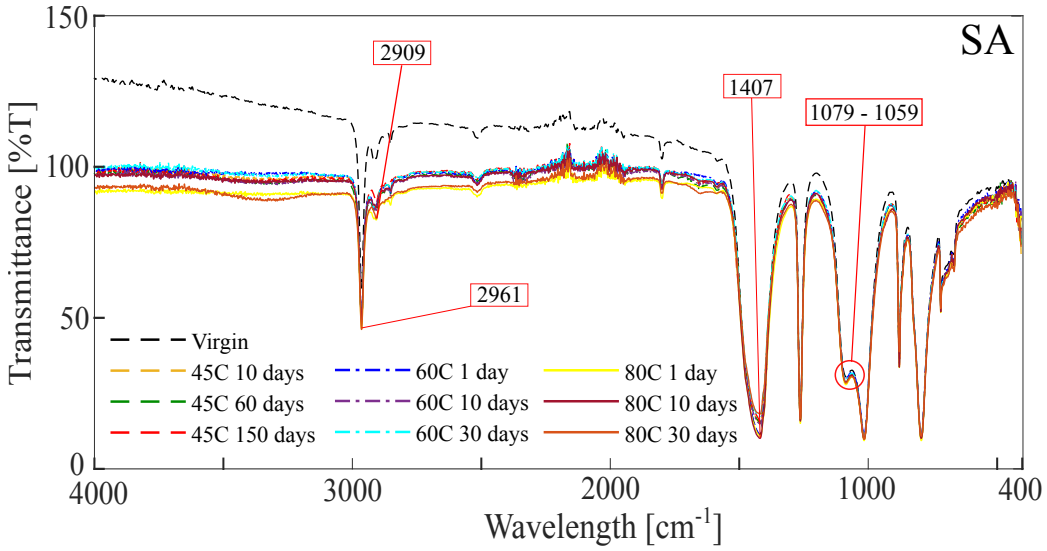


Figure 19: FTIR scan of SA aged at 45°C, 60°C, 80°C for different durations imposed over an unaged sample results.

### 3.4.1. Silicon polymer

Results across the aging temperatures and durations are fairly consistent, with little to no change in the chemical composition of the SA, but rather a loss in transmittance, signifying a decrease in molecular mobility relative to that of the unaged material. Another notable change occurring consistently is that beyond the first period of exposure to UV radiation, little change is occurring with respect to time in the surface layer of the material.

Table 4: SA FTIR functional groups detected

| **Peak wavelength cm$^{-1}$** | **Functional group** | **Movement type** |
|---|---|---|
| 1079 - 1059 | Si-O | stretching |
| 1407 | B-N | Stretching |
| 2909 | C-H (Aldehyde) | stretching |
| 2961 | C-H (Cyclic Alkanes) | Stretching |

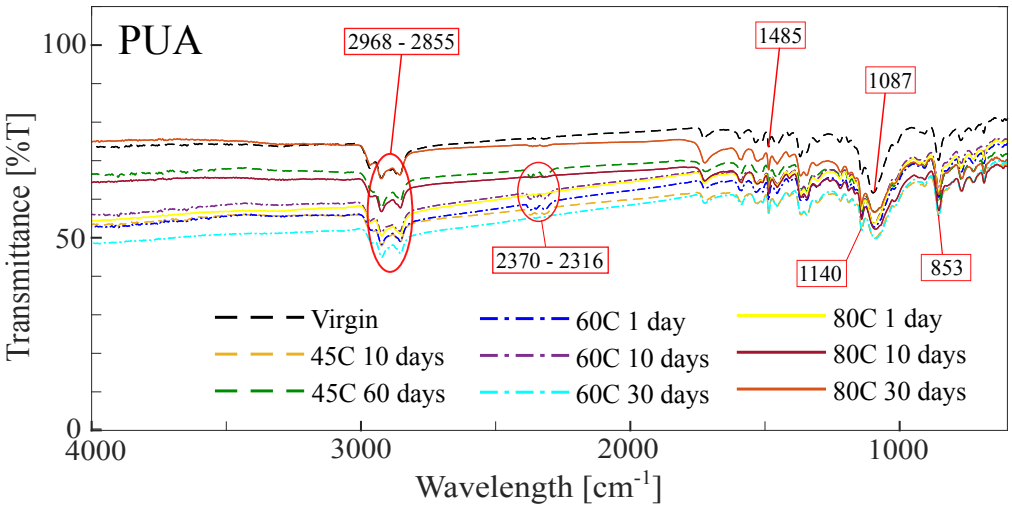


Figure 20: FTIR scan of PUA aged at 45°C, 60°C, 80°C for different durations,imposed over an unaged sample scan

**PUA**

The spectral response of the polyurethane samples varies across the aging periods and temperatures, however a consistent observation is the initial drop in transmittance followed by an increase with respect to time. This phenomena is consistent across all temperatures, but falls short at 60°C, as the transmittance level for the sample aged for 30 days drops again.

Table 5: PUA FTIR functional groups detected

| **Peak wavelength $cm^{-1}$** | **Functional group** | **Movement type** |
|---|---|---|
| 853 | Si-O | stretching |
| 1087 | B-N | Stretching |
| 1140 | C-H (Aldehyde) | stretching |
| 1485 | C-H (Cyclic Alkanes) | Stretching |
| 2316-2370 | C-H (Cyclic Alkanes) | Stretching |
| 2855-2968 | C-H (Cyclic Alkanes) | Stretching |

From a general point of observation, both materials same to be undergoing the same phenomena, which is curing, caused by the breakdown and/or creation of new crosslinks which form the

aged polymeric matrices. This phenomena however only translates to the mechanical behavior at lower temperatures, as higher temperatures cause the materials to soften and weaken with time. This deterioration in performance is not accompanied however with any significant change in functional groups, which further supports the idea that the c-c backbone chains do not experience any significant deterioration or scission from the environmental stresses they were subjected to. thus it is logical to conclude that the change that occurs in the material is mostly due to physical bonding between the chains such as hydrogen bonds (He et al., 2004), as they would not appear with distinctive peaks on the IR scan(Pretsch et al., 2000). Given that the backbones of the polymers are indeed intact and no complications are occurring in the chemical structure of the materials, we can safely assume that even though the damage caused by the environmental and mechanical factors would operate on the same fronts, which is the current state of crosslinks developed in the material with little effect on the main chains. This means that with our experiments we can can isolate the compounding factors from each of these modes of damage in the constitutive behavior and use it to characterize the constitutive behavior of the materials.

## 3.5. DSC test

The DSC test was conducted on aged sampled of both materials providing us with an insight on the change in their heat properties throughout the aging process. Figure 22 and 24 show the variation in Heat capacity of both materials across different temperatures.

The behavior of SA ad PUA in the DSC test show initial variation in the heat capacity either increase or decrease. The extent of this variation however drops along the aging period and approaches that of the unaged material. This shows that regardless of whether either material shows a change in it's microstructural configuration causing it to be able to absorb more or less heat, the final configuration achieved cannot vary significantly from the main configuration seen in the primary chain and cross-link assortment which gives each material its basic physical characteristics.

considering that the heat flow varies directly with heat capacity according to the following

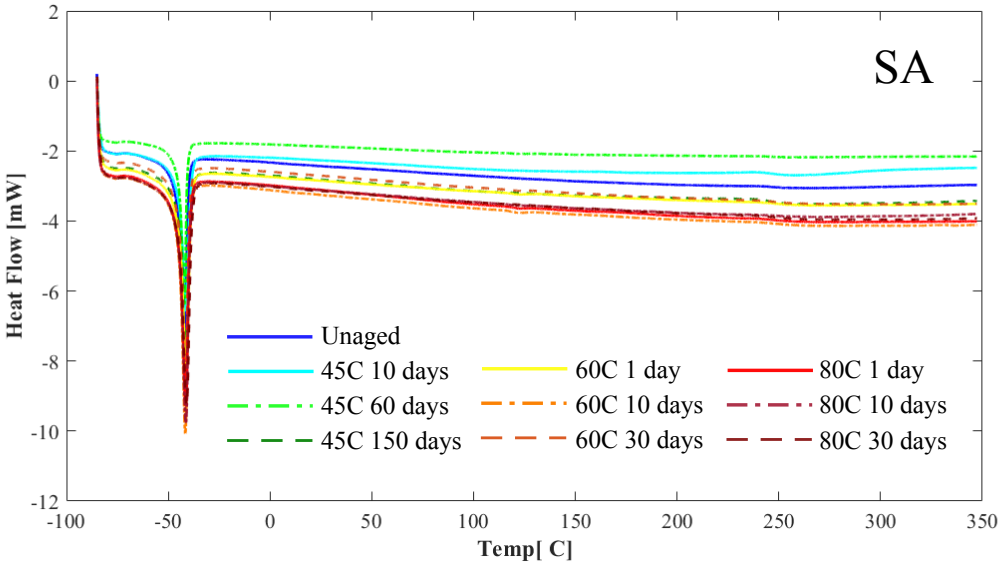


Figure 21: Heat flow plot generated from DSC scan of SA aged at 45°C, 60°C, 80°C for different durations imposed over an unaged sample results.

equation:

$$\frac{dH}{dt} = Cp\frac{dT}{dt} + f(T,t) \tag{5}$$

Where dH/dt is the heat flow, Cp is the heat capacity and $f$(T,t) is a function of Heat Flow due to Kinetic Processes. Considering that the heat flow and capacity mirror each other in both materials, we are able to deduce that the heat flow due to kinetic processes changes according to time and temperature in a similar manner for both materials.

The change of the *Endothermic Melting Temperature* of SA along the aging period is presented in Figure 25 a) and shows that the temperature fluctuates marginally along the aging process. This indicates that the physical bods that maintain the solid state of the polymer become marginally stronger. This is supported by the results of the tensile tests, which show that there is an increase in stiffness for the material along the aging durations.

The *Glassification temperature* of PUA along the aging duration is presented in Figure 25 b) and shows that the temperature generally shows an initial rise, however this is followed by a decline for longer aging durations. It is apparent from the rest of the data presented in this

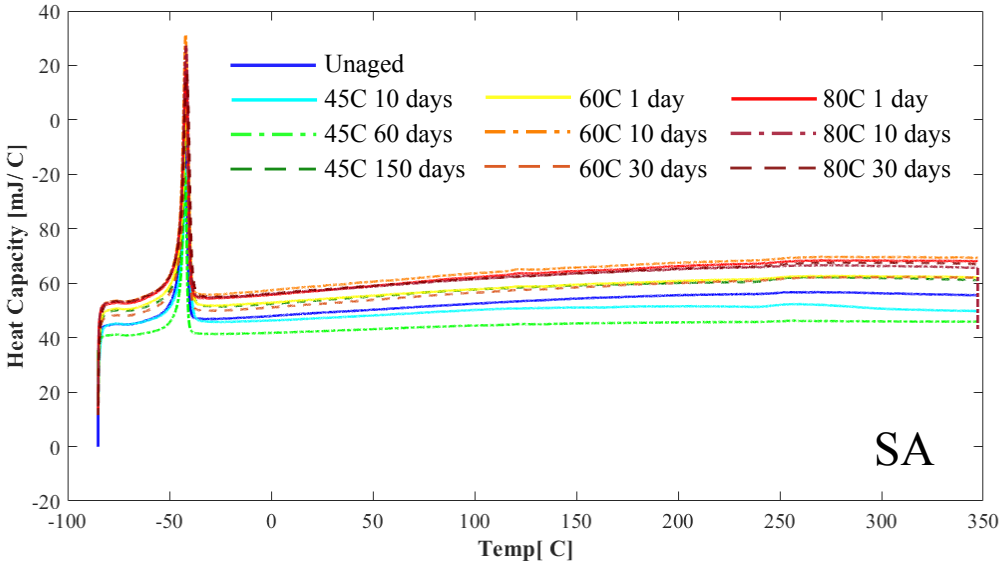


Figure 22: Heat capacity plot generated from DSC scan of SA aged at 45°C, 60°C, 80°C for different durations imposed over an unaged sample results.

study that the micro-structural evolution at the 30 days of aging is different at 60°C than the other two temperatures of the study. The trend of decline in micro-structural integrity due to the environmental damage sustained from aging is apparent in the presented data, as any enhancement in micro-structural integrity during the over-curing phase is overridden by the damage accumulated from aging in the long run.

## 3.6. Swelling test

The swelling test is performed to describe the changes in the cross-link density throughout the course of aging by measuring the amount of swelling of each compound in its Hexane, Toluene and Pentane solvents using the following equation:

$$\frac{n_e}{V_0} = \frac{\rho}{M_x}\left(1 - \frac{2M_x}{M}\right), \tag{6}$$

where $n_e$ is the molar cross-linking, $V_0$ is the starting volume of the elastomer, $\rho$ is the density of the solvent, $M_x$ is the molar volume of the solvent and $M$ is the molar volume of the elastomer(Flory,

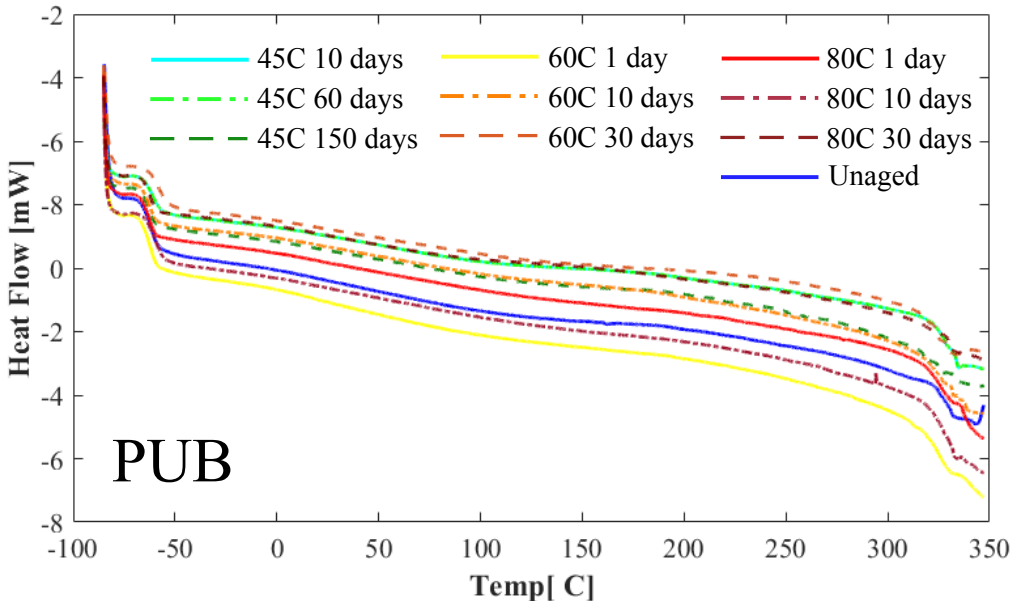


Figure 23: Heat flow plot generated from DSC scan of PUA aged at 45°C, 60°C, 80°C for different durations imposed over an unaged sample results.

1953, Hiemenz and Lodge, 2007, Rubinstein and Colby, 2003). The response of the materials varies with respect to different solvents; SA showed a clear swelling response to all three solvents, with Hexane being the most clear and consistent response across the samples. PUA however, did not respond well to both Hexane and Pentane, but showed marginal swelling with Toluene, which is represented in Figure 26

Samples exhibit different behaviors in the test, where the cross-link density of SA marginally increases and reaches a stabilized plateau after a certain time. Such a plateau in cross-linking cannot be correlated directly with either the stiffening or softening behavior of the material across the aging temperatures, given that the level of cross-linking does not rise and fall with the mechanical behavior. This along with considering that cross-linking is primarily a product of the environmental stress, we can deduce that the mechanical behavior is dependent on other factors than the products of the environmental damage that occurs in the material.

The behavior of PUA marginally varies across both aging period and time, however at $45^{o}$C the behavior is that of an initial increase in cross-linking until a certain peak level, beyond which

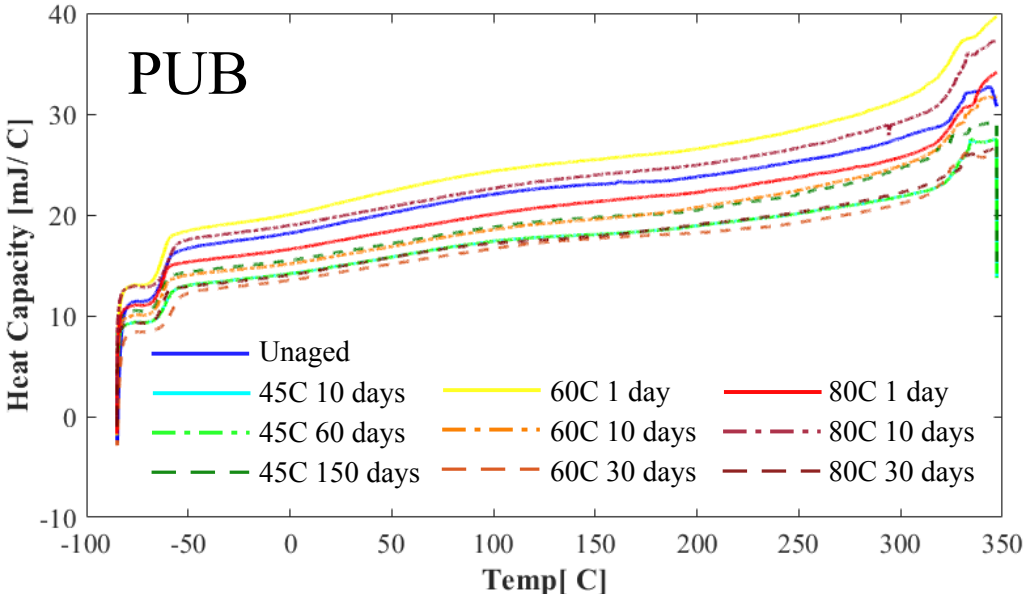


Figure 24: Heat capacity plot generated from DSC scan of PUA aged at 45°C, 60°C, 80°C for different durations imposed over an unaged sample results.

a steady decrease is observed. Thermo-oxidation does not seam to affect the development of cross-links in SA and accordingly it can be assumed that the role of thermo-photo-oxidation on PUA is comparatively greater from a micro-structural standpoint than on SA. On the other hand, thermo-photo-oxidation has varying effects on PUA, however across all aging temperatures and with longer aging durations, cross-link density drops from the peak values that are reached in the over-curing period of aging. This being the case, it is more challenging to separate the exact environmental effects of both photo-oxidation and Thermo-photo-oxidation in the case of the PUA.

The results shown in Figure 26 also indicate that there isn't a proper correlation between the constitutive behavior of the materials and the density of crosslinks, as both of the results do not follow each other in their increasing and decreasing values. This leads to the conclusion that even though the crosslinks have a role to play in the constitutive behavior of the materials, it is indeed their type, how they are bonded to the polymer chains, the length and amount of chains and the micro-structure which they create that collaboratively have the main influence on the mechanical behavior. Thus the contribution of each factor must be considered from a qualitative perspective

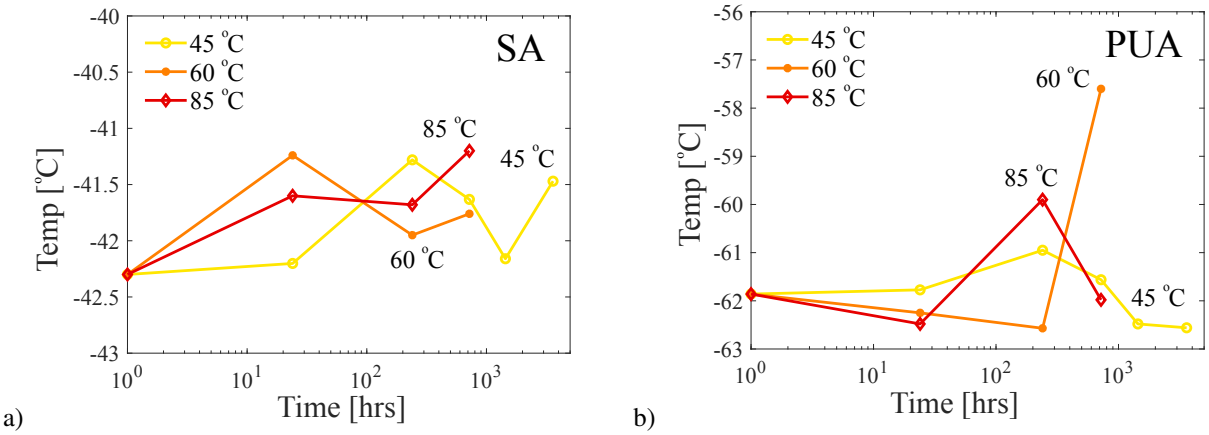


Figure 25: Change in a) Endothermic melting temperature for SA and b) glassification temperature for PUA at 45°C, 60°C, 80°C for different aging durations

rather than a quantitative one.

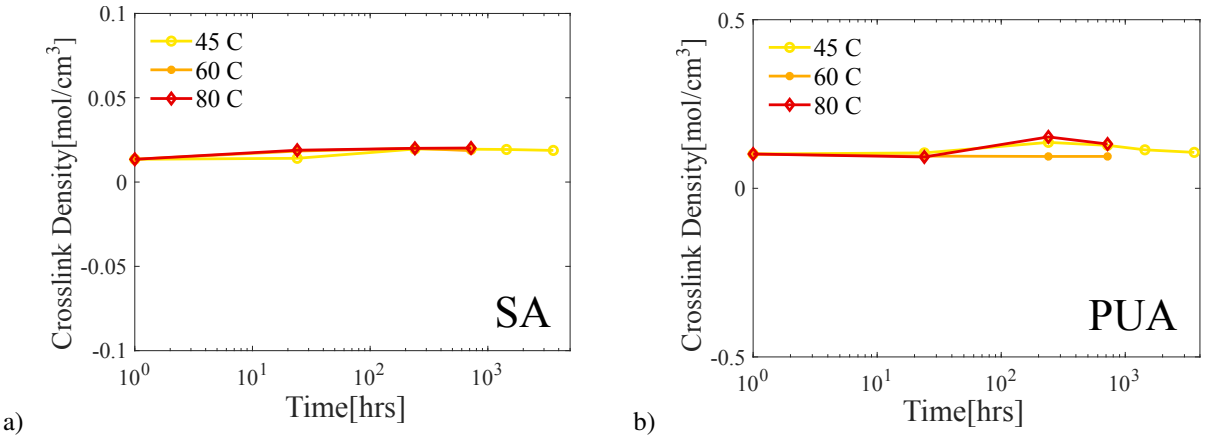


Figure 26: Cross-link density of a) SA and b) PUB elastomers at 45°C, 60°C, 80°C for different durations

## 4. MODELLING

For modelling the behavior of the material a simple Neo-Hookean model based on Gaussian theory was used to represent the response of the material to tensile(James and Guth, 1943)(Rezig et al., 2020). The formulation of equation.8 is centered around the cross-link density of the material as the defining parameter which accounts for the effects of aging which include time, temperature and UV radiation.

$$M_c = \frac{1}{2V_c} \tag{7}$$

$$\sigma = (\frac{\rho RT}{M_c})((P(1 - \frac{2}{f})(\lambda - \frac{1}{\lambda}))^n) \tag{8}$$

where $M_c$ is the mass density of the rubber, $V_c$ the cross-link density,$\sigma$ the stress response of the material measured in MPa, R being the gas constant, T being the aging temperature,$P$ is a multiplicative factorial, $f$ the functionality of the crosslinks for each specific material, $n$ the stress factorial and lambda being the strain the material is subjected to. The factorials were adjusted to fit the unaged behavior of both materials and were maintained at those values for all other plots.

Accordingly the projected compared to the experimental values of the stress were plotted for strains up 300% as represented in Figure 27 for SA and in Figure 28 for PUA.

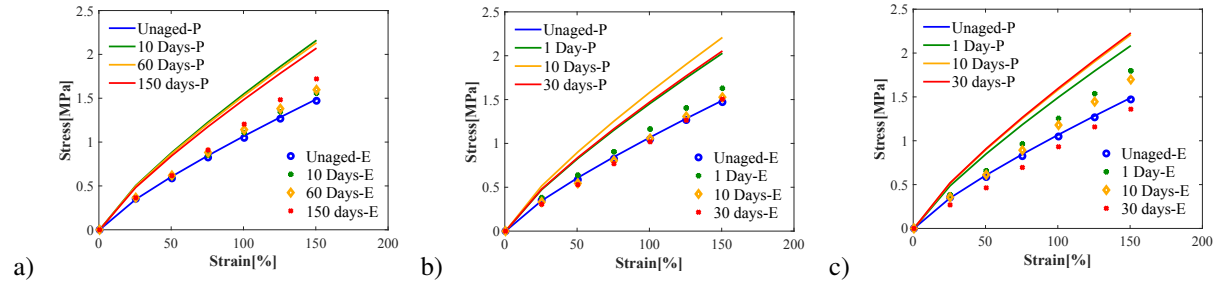


Figure 27: Results of the a) Projected(P) results of the failure test vs the Experimental(E) results for the SA material at 45°C, b) 60°C, and c) 80°C for different aging periods.

Considering that the Neo-hookean model is dependant on the variation in cross-link density as

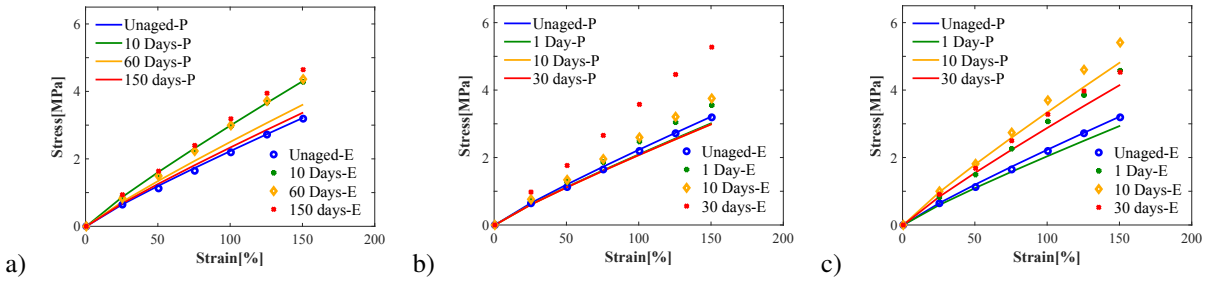


Figure 28: Results of the a) Projected(P) results of the failure test vs the Experimental(E) results for the PUA material at 45°C, b) 60°C, and c) 80°C for different aging periods.

the parameter for mechanical behavior representation, it is of little surprise that the experimental results do not match the projected results of the model. The stress-strain values generated experimentally show a drop in stiffness along the aging process, which is not mirrored by the values of the cross-link density and accordingly not mirrored by the projected plot. This further illustrates the separation between the mechanical and environmental damage modes, given that the mechanical mode is clearly not reliant on the most prominent parameter of the environmental damage, i.e the cross-link density.

## 5. SIGNIFICANCE IN MODELLING

The collected data allowed the study of a relationship between energy dissipation, cyclic stress and permanent set for both constant- and incremental-amplitude regimes. Results showed clear possibility of decomposition of mechanical $D_{mech}$ and environmental damages $D_{env}$ in most cases and with respect to most factors considered for characterization; the increase in accumulated energy happened at later stages of cyclic loading, supporting our earlier findings. The presented graphs can be extremely useful for modeling of aging in soft materials, by serving as a reference to describe the error in the multiplicative decomposition of mechanical and environmental damages which plays a critical factor in simplifying the modeling approach. According to the previous results, one can safely assume that the constitutive behavior of the samples can be modeled using classical representation of accumulative damage factor $D$ where

$$\Psi_N = (1 - D)\,\Psi_0, \qquad D \approx D_{env} D_{mech} \tag{9}$$

where $\Psi_N$ represents the energy of the aged matrix, and $\Psi_0$ represents the energy of virgin material.

This can serve as a functional alternate route to the shape-function reliant micro-mechanical approach presented in (Mohammadi et al., 2020), which relies on defining the aged material's behavior by interpolating between the behavior of the unaged network and that of a fully damaged network as presented in the following equation.

$$\Psi_N = S_0 \Psi_0 + S_\infty \Psi_\infty, \tag{10}$$

where $\Psi_N$ represents the energy of the aged matrix, $\Psi_0$ and $S_0$ represent the shape function and the energy of virgin material. $\Psi_\infty$ and $S_\infty$ represent the shape function and the energy of fully aged material.

The damage factor approach can additionally be utilized to complement the shape-function and

further define the behavior of the fully damaged network, increasing the accuracy and reliability of the final prediction.

# 6. CONCLUSION

Considering that both materials used for this study share similar behavior in their cured unaged condition, it is not unexpected that their behavior with aging on both the mechanical and chemical fronts do not differ significantly. It has been shown in this study that the modes of damage that the materials exhibit can indeed be separated into environmental and mechanical components, both of which operate through the polymer chains and their cross-links which holds and fold the chains together. With the environmental damage occurring mainly in the crosslinked network in comparison to the mechanical network. Considering that both modes of damage are separable we can deduce that the chains and links within the matrix of the material would have different configurations, which cause them to be affected differently according to the stresses they are subjected to. We are also able to further breakdown the environmental mode of damage into two distinct components, that caused solely by photo-oxidation and that caused by the combination of photo and thermo-oxidation. Upon isolating the exact effects of mechanical and environmental damages on the individual networks they act on, we would be able to combine these factors into a micro-mechanical model to properly predict the constitutive behavior of elastomeric materials subjected to the combined weathering conditions found in applications subjected to solar radiation.

# REFERENCES

# REFERENCES


S. Al-Azhary, H. Mohammadi, and R. Dargazany. Thermo-oxidation analysis of structural adhesives: An experimen- tal study. In ASME 2020 International Mechanical Engineering Congress and Exposition. American Society of Mechanical Engineers, 2020.

A. B. S. Andrew R. George. A new spectroscopic method for the non-destructive characterization of weathering damage in plastics. (English) [On weathering of polymers]. *Journal of Advanced Materials*, 40(2):41–56, 2008.

L. Audouin, S. Girois, L. Achimsky, and J. Verdu. Effect of temperature on the photooxidation of polypropylene films. Polymer degradation and stability, 60(1):137–143, 1998.

A. Bahrololoumi, V. Morovati, and R. Dargazany. Hydrolytic aging in rubber-likes materials: Micro-mechanical approach to modeling. International Journal of Plasticity, 1, 2019 (in submission).

A. Bahrololoumi, V. Morovati, E. A. Poshtan, and R. Dargazany. A multi-physics constitutive model to predict quasi-static behaviour: Hydrolytic aging in thin cross-linked polymers. International Journal of Plasticity, page 102676, 2020.

Z. Bettina, N. Christophe, S. Christian, and P. Wulff. Chemistry, polymer dynamics and mechanical properties of a two-part polyurethane elastomer during and after crosslinking. Part I: dry conditions. (English) [On crosslinking of polymers]. Polymer, 115(1):77–95, 2017. doi: https://doi.org/10.1016/j.polymer.2017.03.020.

S. Bhatia. *Advanced renewable energy systems,(Part 1 and 2)*.

D. Bigg. Mechanical properties of particulate filled polymers. Polymer Composites, 8(2):115–122, 1987.

M. Biron. Material Selection for Thermoplastic Parts: Practical and Advanced Information. William Andrew, 2015.

A. Blaustein and C. Searle. *Encyclopedia of Biodiversity (Second Edition), Ultraviolet Radiation*. Academic Press, 2013.

D. Bower. *An Introduction to Polymer Physics*. Cambridge, 2002.

M. C. Celina. Review of polymer oxidation and its relationship with materials performance and lifetime prediction. Polymer Degradation and Stability, 98(12):2419–2429, 2013.

R. Chandra and R. Rustgi. Biodegradable polymers. 23:1273–1335.

J. Cruz-Pinto, M. Carvalho, and J. Ferreira. The kinetics and mechanism of polyethylene photo-oxidation. *Die Angewandte Makromolekulare Chemie: Applied Macromolecular Chemistry and Physics, 216(1):113–133, 1994.*

A. Dupuis, F.-X. Perrin, A. U. Torres, J.-P. Habas, L. Belec, and J.-F. Chailan. Photo-oxidative degradation behavior of linseed oil based epoxy resin. Polymer Degradation and Stability, 135:73–84, 2017.

D. Feldman. Polymer Weathering: Photo-Oxidation. (English) [On photo-oxidation of polymers]. Journal of Polymers and the Environment, 10(1):163–173, 2002. doi: https://doi.org/10.1023/A:1021148205366.

P. Flory. Principles of polymer chemistry. Cornell University Press, 1953.

G. Geuskens and C. David. The photo-oxidation of polymers. a comparison with low molecular weight compounds. In Photochemistry–7, pages 233–240. Elsevier.

K. T. Gillen, M. Celina, R. L. Clough, and J. Wise. Extrapolation of accelerated aging data-arrhenius or erroneous? Trends in polymer science, 8(5):250–257, 1997.

K. T. Gillen, M. Celina, and M. R. Keenan. Methods for predicting more confident lifetimes of seals in air environ-ments. Rubber chemistry and technology, 73(2):265–283, 2000.

Y. He, B. Zhu, and Y. Inoue. Hydrogen bonds in polymer blends. Progress in Polymer Science, 29(10):1021–1051, 2004.

P. C. Hiemenz and T. R. Lodge. Polymer Chemistry, Second Edition. CRC Press, 2007.

H. James and E. Guth. Theory of the elastic properties of rubbers. Journal of Chemical Physics, 11:455, 1943.

F. Khabbaz, A.-C. Albertsson, and S. Karlsson. Chemical and morphological changes of environmentally degradable polyethylene films exposed to thermo-oxidation. Polymer Degradation and Stability, 63(1):127–138, 1999.

Q. Liu, H. Yang, J. Zhao, S. Liu, L. Xia, P. Hu, Y. Lv, Y. Huang, M. Kong, and G. Li. Acceleratory and inhibitory effects of uniaxial tensile stress on the photo-oxidation of polyethylene: Dependence of stress, time duration and temperature. Polymer, 148:316–329, 2018.

L. W. McKeen. The effe ct of sterilization on plastics and elastomers. William Andrew, 2018.

H. Mohammadi and R. Dargazany. Thermo-oxidative aging. Tire Technology Review, pages 54–57, 2018.

H. Mohammadi and R. Dargazany. A micro-mechanical approach to model thermo-oxidative aging in elastomers. International Journal of Plasticity, 118:1–16, 2019.

H. Mohammadi, V. Morovati, E. Poshtan, and R. Dargazany. Understanding decay functions and their contribution in modeling of thermal-induced aging of cross-linked polymers. Polymer Degradation and Stability, page 109108, 2020.

M. Nachtane, M. Tarfaoui, S. Sassi, A. El Moumen, and D. Saifaoui. An investigation of hygrothermal aging effe cts on high strain rate behaviour of adhesively bonded composite joints. Composites Part B: Engineering, 172:111–120, 2019.

H. Namazi. Polymers in our daily life. (English) [On applications of polymeric materials ]. Bioimpacts, 7(2):73–74, 2017. doi: https://bi.tbzmed.ac.ir/FullHtml/bi-17438.

J. E. Pickett. An unusual photo-oxidation pathway for a poly (2, 6-dimethyl-1, 4-phenylene oxide) model compound part a polymer chemistry. 2017.

E. Pretsch, P. B¨uhlmann, C. Affo lter, E. Pretsch, P. Bhuhlmann, and C. Affo lter. Structure determination of organic compounds. Springer, 2000.

A. Quintana and M. C. Celina. Overview of dlo modeling and approaches to predict heterogeneous oxidative polymer degradation. Polymer Degradation and Stability, 149:173–191, 2018.

N. Rezig, T. Bellahcene, A. Aberkane, and A. N. Abdelaziz. Thermo-oxidative ageing Af a Abr rubber: effects An mechanical and chemical properties. Journal of Polymer Research, 27(11):1–13, 2020.

A.Rodriguez, B. Mansoor, G. Ayoub, X. Colin, and A. Benzerga. Effect of uv-aging on the mechanical and fracture behavior of low density polyethylene. Polymer Degradation and Stability, page 109185, 2020.

M.Rubinstein and R. H. Colby. Polymer physics. OUP Oxford, 2003.

M. H. Sadd. Continuum Mechanics Modeling of Material Behavior. Academic Press, 2018.

A. W. Signor, M. R. VanLandingham, and J. W. Chin. Effe cts of ultraviolet radiation exposure on vinyl ester resins: characterization of chemical, physical and mechanical damage. Polymer degradation and stability, 79(2):359–368, 2003.

A. Standard. D412-06 standard test methods for vulcanized rubber and thermoplastic elastomers–tension. ASTM International, West Conshohoken, PA, USA, 2006.

A. Standard. G151-19 standard practice for exposing nonmetallic materials in accelerated test devices that use labo-ratory light sources. ASTM International, West Conshohoken, PA, USA, 2019.

M. Tolinski. Additives for polyolefins: getting the most out of polypropylene, polyethylene and TPO. William Andrew, 2015.

H. Wu, Y. Zhao, X. Dong, L. Su, K. Wang, and D. Wang. Probing into the microstructural evolution of isotactic polypropylene during photo-oxidation degradation. Polymer Degradation and Stability, page 109434, 2020.

M. Zaghdoudi, A. K¨ommling, M. Jaunich, and D. Wolff. Erroneous or arrhenius: A degradation rate-based model for epdm during homogeneous ageing. Polymers, 12(9):2152, 2020.